



Enhanced acetone-sensing properties of Pt-decorated Al-doped ZnO nanoparticles



Aran Koo¹, Ran Yoo¹, Sung Pil Woo, Hyun-Sook Lee*, Wooyoung Lee*

Department of Materials Science and Engineering, Yonsei University, 50 Yonsei-ro, Seodaemun-gu, Seoul, 03722, Republic of Korea

ARTICLE INFO

Keywords:

Al-doped ZnO
Pt decoration
Acetone
Spillover effect
Catalytic effect
Gas sensor

ABSTRACT

We report the excellent sensing performance of Pt-decorated Al-doped ZnO (Pt-AZO) nanoparticles (NPs) for the detection of the hazardous gas, acetone. The Pt NPs were uniformly deposited on the surface of the Al-doped ZnO (AZO) NPs via magnetron sputtering under agitation. The Pt-AZO NPs show remarkably enhanced sensing properties with a sensing response and response time of 421 and 2.9 s, respectively, under exposure to 10 ppm acetone at 450 °C, as compared with those of pure ZnO NPs (17 and 51 s, respectively), AZO NPs (56 and 15 s, respectively), and Pt-decorated ZnO (Pt-ZnO) NPs (261 and 7 s, respectively) under the same conditions. Furthermore, the Pt-AZO NPs showed the highest sensing response to 10 ppm acetone compared to those reported so far for metal-oxide sensing materials. Pt NPs played a crucial role in improving the gas sensing performance of AZO NPs. The catalytic effect of Pt NPs led to a greater number of adsorbed oxygen ion species on the surface of the Pt-AZO NPs, as indicated by the increased number of oxygen vacancies, higher carrier concentration, larger specific surface area, and enhanced reaction kinetics. The outstanding sensing performance of the Pt-AZO NPs as compared to those of pure ZnO, AZO, and Pt-ZnO NPs is attributed to these synergistic effects.

1. Introduction

Large amounts of hazardous gases, such as acetone, benzene, toluene, ammonia, and so on, are released into the atmosphere as by-products of industrialization, causing environmental pollution and posing risks to human health. In particular, acetone, which is very volatile, is used extensively in laboratories and industrial applications [1]. At concentrations higher than 173 ppm, acetone can cause irritation to the eyes, nose, throat, skin, and central nervous system [1,2]. Moreover, it has been known that accidental intake of large amounts of acetone might lead to unconsciousness and death [3]. In addition, acetone is found in the exhaled breath of diabetes patients and can thus be used as a biomarker to determine diabetes [4,5]. The acetone concentration in the exhaled breath of diabetes patients is found to exceed 1.8 ppm, which is higher than that (0.3–0.9 ppm) of healthy people [6,7]. Therefore, the development of gas sensors for the rapid and selective detection of acetone has attracted substantial interest in recent years.

To detect acetone in air, several techniques such as gas chromatography and mass spectrometry have been used. However, these

instruments are bulky, expensive, and cannot be used to perform in situ and continuous measurements. Therefore, use of sensors based on semiconducting metal-oxides, such as SnO₂, WO₃, and TiO₂, has recently been considered as an alternative approach for detecting acetone [8]. Among various sensing materials, ZnO has been extensively investigated as a particularly promising candidate owing to its special characteristics such as low cost, simplicity of preparation, high chemical and thermal stability, and favorable sensing properties. Many experimental studies have been focused on improving the sensing properties of ZnO by designing various structures such as thin films [9], nanorods [10], nanowires [11], nanosheets [12], nanotubes [13], and nanoparticles [14]. However, these structurally modulated ZnO materials exhibit insufficient sensing properties such as a low response, long response time, and lack of selectivity.

To overcome these shortcomings, loading of noble metal (Au [15] and Pt [16]) and doping of transition metals (Cd, Cr, Mn, Fe, Co, and Ni [17–19]) was carried out to enhance the sensing properties of ZnO for acetone detection. Loading of a noble metal loading improves the sensing properties by allowing its catalytic effect to lower the activation energy of the sensing material (ZnO) so that it reacts better with

Abbreviation: AZO, Al-doped ZnO; SEM, scanning electron microscopy; XPS, X-ray photoelectron spectroscopy; XRD, X-ray diffraction; EDS, energy-dispersive X-ray spectroscopy

* Corresponding authors.

E-mail addresses: h-slee@yonsei.ac.kr (H.-S. Lee), wooyoung@yonsei.ac.kr (W. Lee).

¹ These authors contributed equally.

<https://doi.org/10.1016/j.snb.2018.10.049>

Received 19 March 2018; Received in revised form 21 September 2018; Accepted 8 October 2018

Available online 10 October 2018

0925-4005/ © 2018 Elsevier B.V. All rights reserved.

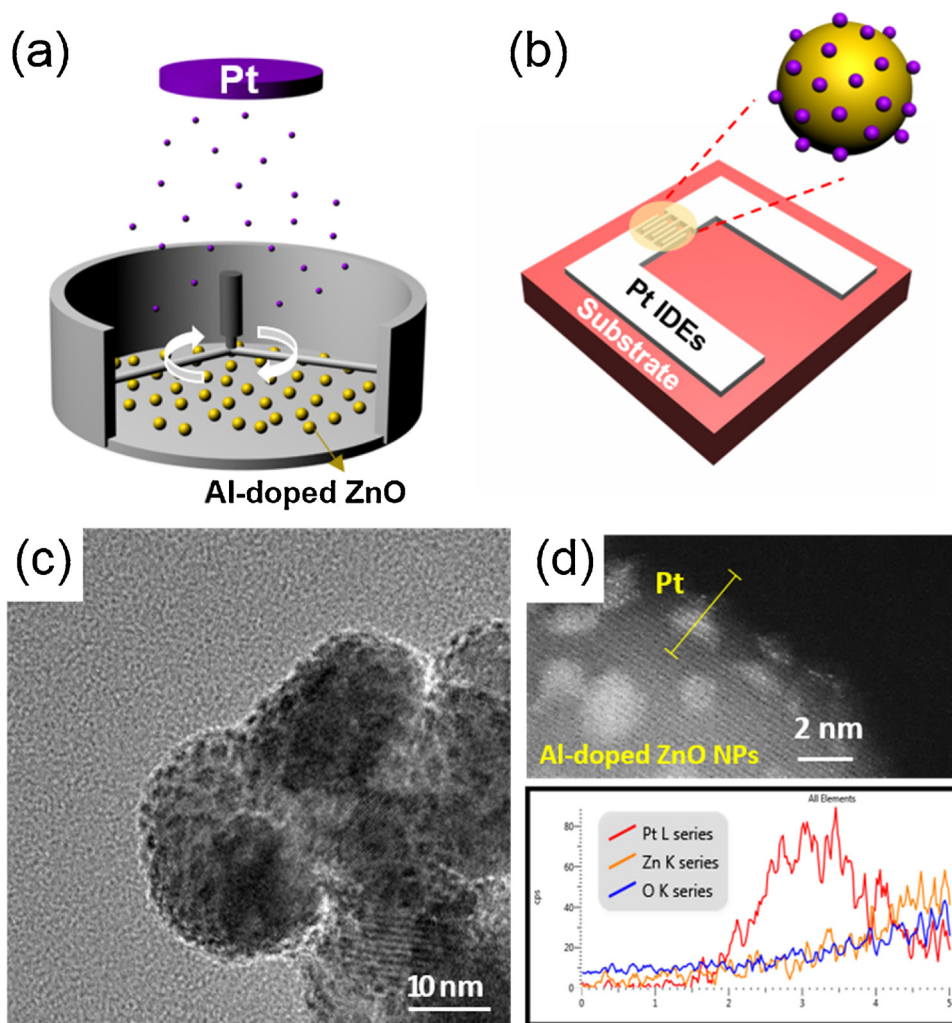


Fig. 1. (a) Schematic of the apparatus used for decorating Pt nanoparticles on AZO particles, (b) schematic of an actual sensor device composed of Pt electrodes on a SiO_2 substrate, (c) high-resolution TEM image of Pt-AZO, and (d) STEM-HAADF image with EDS line profile of an isolated Pt-AZO NP.

acetone. However, according to a previous study [20], using a deposition method to prepare a catalyst does not maximize its efficiency because the noble metal is deposited only onto one side of the sensing material. Further, doping with a third element is another effective way to enhance the gas-sensing properties of the hybrid ZnO material by increasing the number of defects in the crystal structure or changing the electrical properties of the semiconducting metal-oxide. In our previous studies, we improved the acetone-sensing properties of ZnO by doping with transition metals (Al, Co, Cu, Mn) [21,22]. However, further improvement of the performance of acetone gas sensors is required to achieve high sensitivity, short response times, and good selectivity.

In this study, we developed an acetone sensor by decorating Pt NPs on the surface of Al-doped ZnO NPs, to realize improved sensing properties such as high sensing response, rapid response time, and good selectivity. The considerable improvement in the performance was derived from both the inclusion of catalytic particles (a noble metal loading) and doping of a transition metal. Specifically, to maximize the catalytic effect, the Pt NPs were homogeneously decorated over a maximum possible area of the surface of Al-doped ZnO NPs via a new synthetic method (sputtering in an agitated vessel). The acetone-gas-sensing mechanism is discussed in detail using the results of physical and chemical analyses.

2. Experimental

2.1. Synthesis of Pt-decorated Al-doped ZnO NPs

Undoped ZnO NPs and Al-doped ZnO (AZO) NPs were synthesized by a hydrothermal method described in our previous reports [21,22]. In the synthesis of AZO NPs, the concentration of doped Al was maintained at 1 at.%. After the hydrothermal reaction, the synthetic product was collected by centrifugation and washed with methanol. Then, it was dried at 90°C for 60 min and annealed at 350°C for 30 min in a H_2 atmosphere. To synthesize the Pt-decorated Al-doped ZnO (Pt-AZO) NPs, platinum was coated on the surface of the as-synthesized AZO NPs in an agitated vessel for 2 min at a deposition rate of 6–7 nm/min using a DC magnetron sputtering system, as illustrated in Fig. 1(a). The AZO powder was continuously stirred with the help of a rotating impeller and the Pt NPs could be homogeneously decorated on the surface of the AZO NPs. Pt-decorated ZnO (Pt-ZnO) NPs also were prepared by the same method to confirm the catalytic effect of Pt.

2.2. Structural characterization

The structural and elemental characterization of the as-synthesized NPs were carried out using a field-emission transmission electron microscope (FE-TEM, JEOL JEM ARM 200F) equipped with an energy-dispersive X-ray spectroscopy (EDS). The crystal structure was

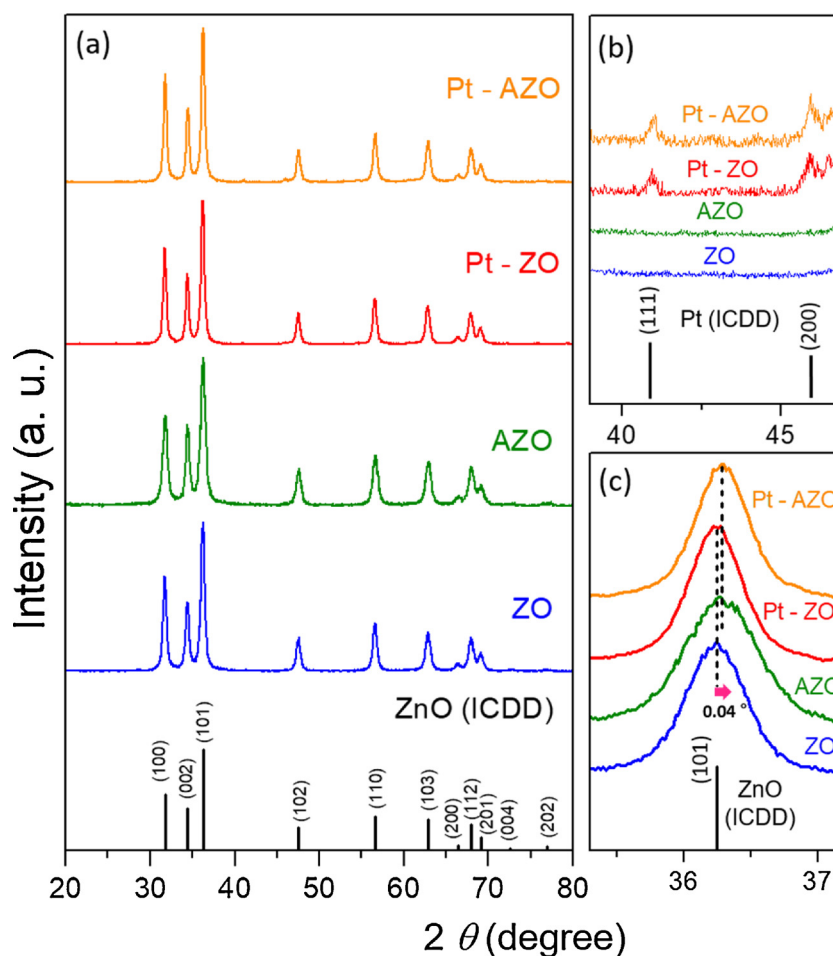


Fig. 2. (a) XRD patterns of pure ZnO, AZO, Pt-ZnO, and Pt-AZO. The standard XRD pattern of hexagonal wurtzite-type ZnO (ICDD: # 98-000-0483) is shown as vertical lines at the bottom, (b) magnified (111) and (200) peaks of the face-centered cubic structures of Pt (ICDD: # 01-087-0636), (c) magnified (101) peak of ZnO.

investigated by X-ray diffraction (XRD, Ultima IV/ME 200DX, Rigaku) using Cu $K\alpha$ radiation. Surface elemental analysis was conducted by X-ray photoelectron spectroscopy (XPS, K-alpha Thermo VG) using Al $K\alpha$ radiation (1486.6 eV) from an X-ray source operating at 12 kV with a current of 3 mA. The optical properties of the ZnO NPs were examined by UV–vis spectroscopy (UV–vis, V-650 JASCO) in the wavelength region of 250–800 nm.

2.3. Fabrication of gas sensor devices and the evaluation of their sensing performance

The sensor devices (8.5 mm × 8.5 mm) were fabricated on an interdigitated Pt electrode, 10 mm wide and 10 mm long separated by a gap of 10 μm , as shown in Fig. 1(b). Cr (20 nm) and Pt (100 nm) layers were deposited on the patterned SiO₂ substrate via a DC magnetic sputtering process. The Cr layer was used as an interlayer to achieve good contact between the Pt layer and the SiO₂ substrate. The synthesized powder was mixed with α -terpineol to form a paste, and the mixture was spread on the interdigitated Pt electrode to serve as the sensing layer. To remove the binding agent and enhance the stability of the sensor, the sensor was dried at 300 °C for 1 h and annealed at 600 °C for another hour.

For the gas-sensing measurements, the sensors were mounted on a chamber and placed in a flow system equipped with gas cylinders and mass flow controllers (MFCs). A mixing of acetone gas and air was controlled by varying the gas flow rates produced by the MFCs. To evaluate the sensing properties, a combination of a current source (Keithley 6220) and a nanovoltmeter (Keithley 2182) was used, and a

constant current of 10 nA was applied for a time interval of 0.1 s. The gas sensing measurements were conducted at operating temperatures between 300 and 500 °C. The sensing response of the sensor for acetone gas is defined as $(R_a - R_g)/R_g$, where R_a and R_g are the resistances of the sensors in air and in an environment containing acetone, respectively.

3. Results and discussion

Fig. 1(a) and (b) schematically illustrate the apparatus used for decorating Pt NPs on AZO NPs and a sensor device based on the synthesized particles, respectively. Fig. 1(c) shows a TEM image of the as-synthesized Pt-AZO NPs, revealing that the Pt-AZO NPs are spherical with a diameter of \sim 20 nm. Fig. 1(d) shows the STEM-HAADF image and EDS line profile corresponding to an isolated Pt-AZO NP marked with a yellow line on the surface of the particle, which reveal the existence of Pt on the AZO NPs and confirm that \sim 2 nm-sized Pt NPs are uniformly distributed on the surface of the AZO NPs.

The phase structure of the ZnO, AZO, Pt-ZnO, and Pt-AZO NPs was characterized by XRD (Fig. 2). The diffraction peaks of all the samples could be indexed to the hexagonal wurtzite ZnO phase (ICDD: # 98-000-0483) (Fig. 2(a)). Further, the (111) and (200) reflections of the face-centered cubic structure of the Pt crystals (ICDD: # 01-087-0636) are observed in the XRD patterns of Pt-ZnO and Pt-AZO NPs (Fig. 2(b)). No other secondary phases or impurity peaks are observed in any of the XRD patterns. The main (101) peak of ZnO is located at the same position in the XRD patterns of both the AZO and Pt-AZO samples, with a slight shift to higher angles by \sim 0.04° compared to those of the

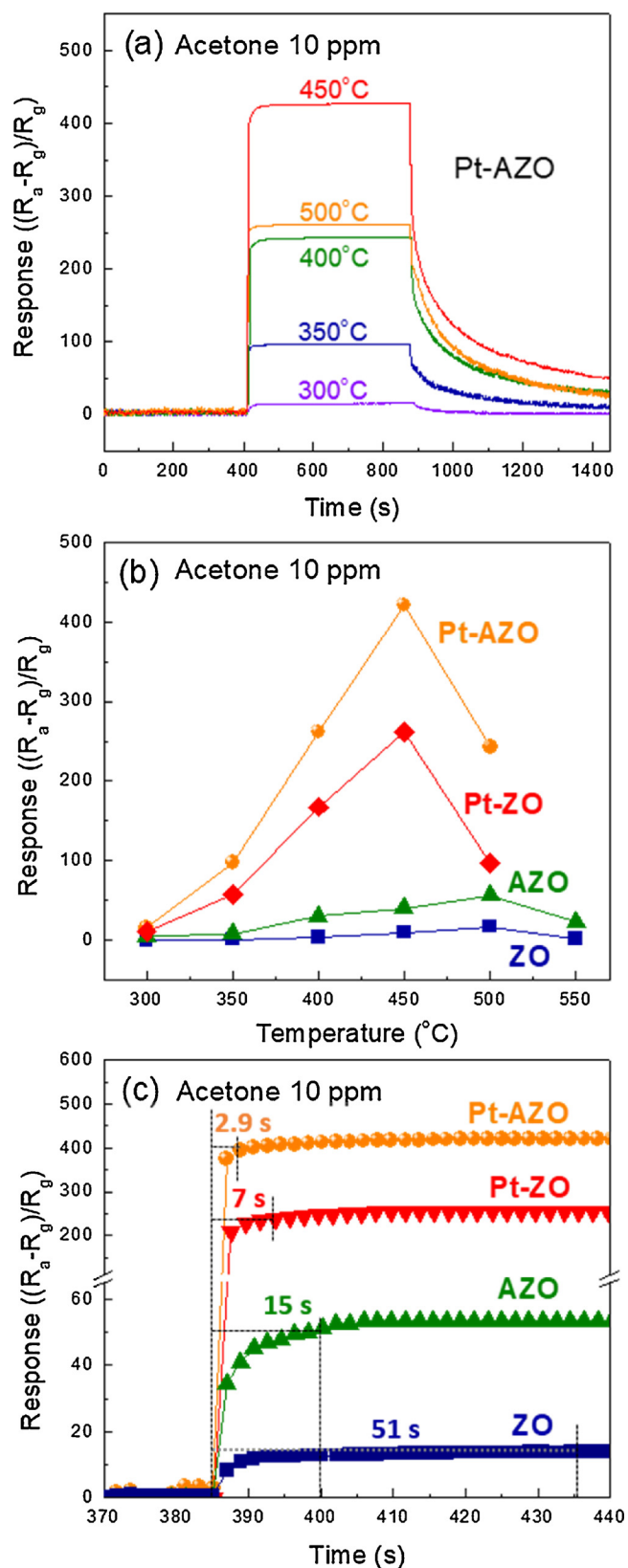


Fig. 3. (a) Variation in the sensing response of Pt-AZO to 10 ppm acetone in the operating temperature range of 300–500 °C, (b) maximum sensing response of ZnO, AZO, Pt-ZnO, and Pt-AZO at 10 ppm acetone as a function of the operating temperature, and (c) the response times of ZnO, AZO, Pt-ZnO, and Pt-AZO.

undoped ZnO and Pt-ZnO NPs (Fig. 2(c)). This shift in the main peak to a higher angle is attributed to the reduction in the interlayer spacing of ZnO along the (101) axis owing to the replacement of Zn^{2+} (atomic radius, 0.74 Å) with Al^{3+} , which has a smaller atomic radius of 0.53 Å. The diffraction peak of Pt-AZO is shifted to the same extent as that of AZO, indicating that the Al dopant is well integrated into the ZnO lattice sites. More importantly, the similar shift implies that Pt is not incorporated into the ZnO lattice but is attached to the surface of AZO in the form of NPs, which is consistent with the NP morphology observed in Fig. 1(c).

The sensing properties of the ZnO, AZO, Pt-ZnO, and Pt-AZO NPs were evaluated under exposure to 10 ppm acetone at different operating temperatures. Fig. 3(a) presents the variations in the responses of the Pt-AZO NPs at different operating temperatures over the 300–550 °C temperature range, and Fig. 3(b) presents the maximum sensing responses of the samples. As shown in Fig. 3(b), the optimal working temperature is 500 °C for ZnO and AZO NPs and 450 °C for Pt-ZnO and Pt-AZO NPs. Above these temperatures, the sensing response decreases, which is attributed to the competing desorption of the chemisorbed oxygen atoms on the surface of the nanoparticles [23]. Further, it is apparent from Fig. 3(b) that the sensing responses of the AZO NPs (~56) and Pt-AZO NPs (~421) are correspondingly higher than those of the ZnO NPs (~17) and Pt-ZnO (~261), respectively. This result implies that Al doping induces an improvement in the sensing response. However, the responses of the Pt-decorated samples are significantly higher than those of the corresponding samples without Pt, indicating that the remarkable enhancement in the sensing response arises due to Pt decoration rather than Al doping. Thus, the sensor based on Pt-AZO NPs shows the highest sensing response among the sensors based on the fabricated samples, at the optimal working temperature of 450 °C.

The response time of the sensors based on ZnO, AZO, Pt-ZnO, and Pt-AZO NPs for 10 ppm acetone is defined as the time required to reach 90% of the total resistance change upon exposure to the test gas and it was estimated from the plots of the response variation as a function of time (Fig. 3(c)). The response times determined thus are 51, 15, 7, and 2.9 s for the ZnO, AZO, Pt-ZnO, and Pt-AZO NPs, respectively, indicating that the response time decreases due to Al doping as well as the incorporation of Pt NPs. The recovery times of the sensors based on ZnO, AZO, Pt-ZnO, and Pt-AZO NPs estimated as the time necessary for the resistance change to reach 90% of the original baseline signal upon the removal of the target gas are approximately 55, 276, 357, and 440 s, respectively. In contrast to the decrease in the response time with Al doping and Pt catalyst incorporation, the recovery times increased. This is attributed to the remaining gas molecules remaining on the detecting surface of the sensing materials after the chemical adsorption reaction of the gas molecules during the sensing procedure. Therefore, a long resting time is required for all these molecules to desorb from the detecting surface. However, further detailed study is required to understand the reason for the slow recovery times of AZO, Pt-ZnO, and Pt-AZO NPs compared to that of ZnO NPs.

Meanwhile, we also investigated the effect of Pt content on the sensing performance of AZO NPs by comparing the sensing responses of sensors based on Pt-AZO NPs prepared with different Pt deposition times, for example, 2 and 4 min. The Pt-AZO, prepared with 2 min deposition time, showed a uniform distribution of Pt NPs with a size of ~2 nm on the surface of AZO (See Fig. 1), whereas the sample prepared with 4 min showed an aggregation and non-uniform distribution of Pt NPs (See Fig. S1). Furthermore, as shown in Fig. S2, the best sensing response was observed for the sensor based on Pt-AZO NPs prepared using a Pt-deposition time of 2 min rather than 4 min, implying that the Pt content on the ZnO surface is a critical parameter determining the sensing performance of such a sensor. The relationship between the Pt coating time and Pt content of the Pt-AZO NPs and additional in-depth studies on the optimal Pt content for achieving the highest sensing performance of AZO NPs to acetone will be carried out in the future.

Fig. 4(a) shows the dynamic response of the sensor based on Pt-AZO

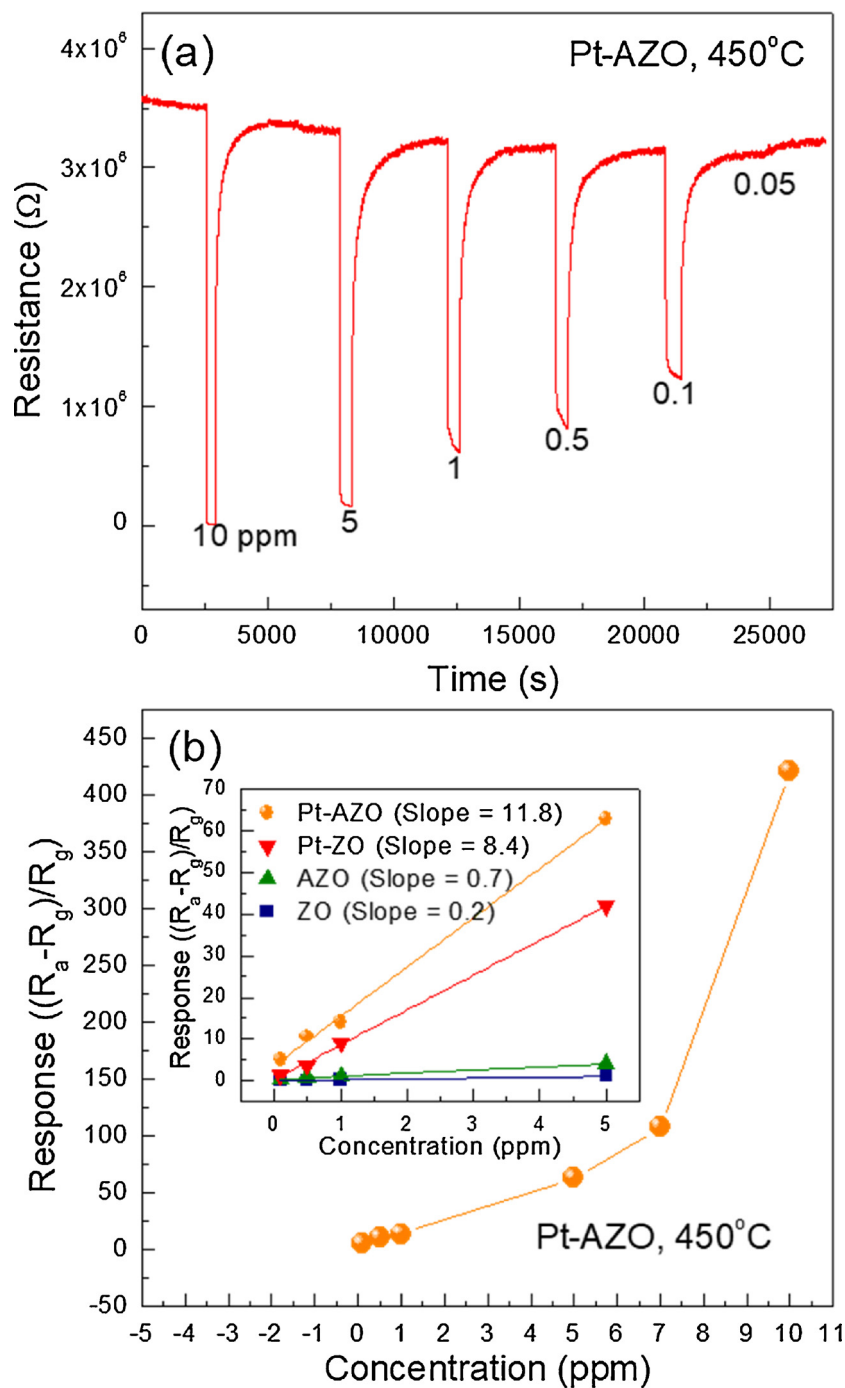


Fig. 4. (a) Variation in the resistance of Pt-AZO during the detection of acetone at different concentrations in the range of 0.05–10 ppm at 450 °C, (b) sensing responses of Pt-AZO to different concentrations of acetone in the range of 0.1–10 ppm at 450 °C. (Inset: sensitivity of ZnO, AZO, Pt-ZnO, and Pt-AZO NPs with calibration curves in the range of 0.1–5 ppm).

NPs for different concentrations of acetone ranging from 0.05 to 10 ppm at 450 °C. The resistance of the Pt-AZO NP sensor decreased with a reduction in the acetone concentration, indicating that the ZnO particles retain their n-type semiconducting properties after Pt decoration and Al doping. Fig. 4(b) shows the response of the Pt-AZO NP sensor at various acetone concentrations in the range of 0.1–10 ppm at 450 °C. The sensing response increases with increasing acetone concentration. The inset of Fig. 4(b) shows that the responses of the sensors based on ZnO, AZO, Pt-ZnO, and Pt-AZO NPs increase linearly as a function of acetone concentration in the range of 0.1–5 ppm, at their optimal operating temperatures. The linear correlation coefficient R^2 in Fig. 4(b) is close to 1, implying good linearity. The estimated

sensitivities of the sensors in the range of 0.1–5 ppm acetone are 0.2, 0.7, 8.4, and 11.8 corresponding to the ZnO, AZO, Pt-ZnO, and Pt-AZO NPs, respectively. Thus, the sensor based on Pt-AZO NPs shows the highest sensitivity among the sensors studied.

The chemical characteristics of the initial state of the ZnO, AZO, Pt-ZnO, and Pt-AZO NPs were investigated by XPS. The XPS O 1s spectra of the samples are shown in Fig. 5. The peaks of O 1s level could be deconvoluted into three quasi-Gaussian peaks centered at approximately 530, 531, and 532 eV. The peak at ~ 530 eV (red line) is associated with the O^{2-} ions of the Zn-O bonds in the wurtzite structure of ZnO, which are thought to be stable and do not contribute to the gas response [24]. The peak at ~ 531 eV (orange line) is attributed to the

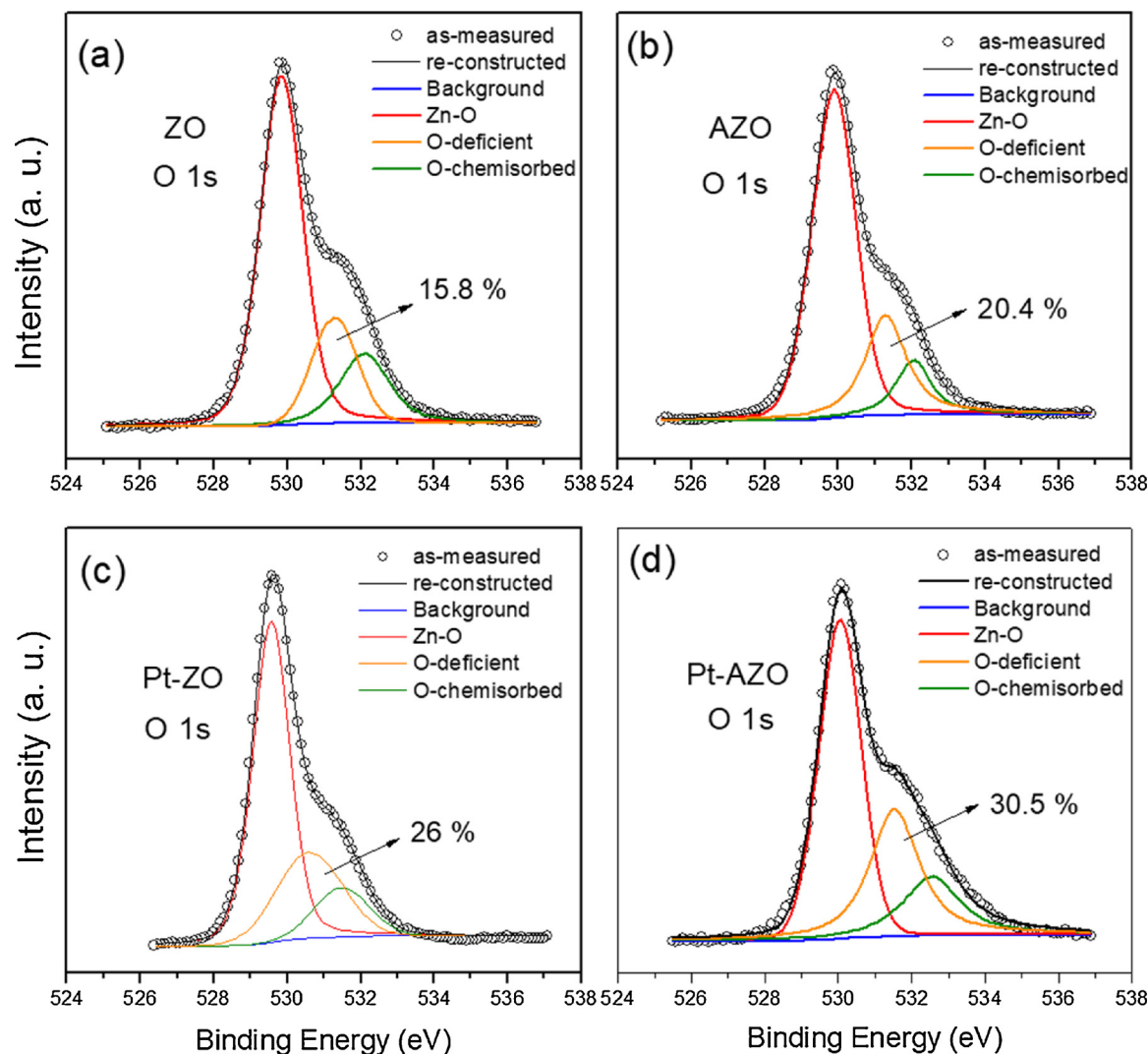


Fig. 5. XPS O 1s spectra of (a) ZnO, (b) AZO, (c) Pt-ZnO, and (d) Pt-AZO.

adsorbed oxygen ions (O^- and O^{2-}), which significantly influence the gas-sensing properties in the oxygen-deficient regions, such as oxygen vacancies and oxygen interstices, within ZnO [24]. The peak intensities partially indicate the variation in the concentration of the oxygen deficiencies. The peak at ~ 532 eV (green line) is assigned to chemisorbed oxygen species, such as the adsorbed H_2O , O_2 , and $-CO_3$ on the surface of ZnO [24]. The concentration of oxygen deficiencies was estimated by calculating the area fraction of the oxygen-deficient peak in the deconvoluted O 1s peaks. The percentages of adsorbed oxygen ions are thus ~ 15.8 , 20.4 , 26 , and 30.5% for ZnO NPs, AZO NPs, Pt-ZnO NPs, and Pt-AZO NPs, respectively.

The electronic states of the ZnO, AZO, Pt-ZnO, and Pt-AZO NPs were characterized by UV–vis spectroscopy. Fig. 6(a) shows the band gap energies of the ZnO, AZO, Pt-ZnO, and Pt-AZO NPs, determined from the UV–vis absorbance spectra shown in the inset of Fig. 6(a). The inset of Fig. 6(a) shows that the absorption peaks of the AZO and Pt-AZO NPs appear at ~ 355 and ~ 365 nm, respectively, which are blue-shifted compared to the peak of pure ZnO located at ~ 371 nm. The blue shift in the absorption peak arises from the Burstein-Moss (BM) effect [25]. Based on the BM model, the Fermi level rises toward the conduction band owing to an increase in the electron carrier concentration and the broadening of the optical band gap. The optical band gap energy (E_g) was determined using the Tauc relation [26]: $ah\nu = C(h\nu - E_g)^n$, where, a is the absorption coefficient, $h\nu$ is the energy of the incident photons, C is a constant, $n = 1/2$ for direct-band-gap semiconductors,

and E_g is the optical band gap. The band gap energies of the ZnO, AZO, Pt-ZnO, and Pt-AZO NPs were determined as the photon energy when $(ah\nu) = 0$ by extrapolating the $[F(ah\nu)^2]$ versus $h\nu$ curve [27] as shown in Fig. 6(a). The optical band gap of the pure ZnO NPs is estimated to be 3.01 eV, whereas those of the AZO, Pt-ZnO, and Pt-AZO NPs are higher at 3.13 , 3.35 , and 3.57 eV, respectively. Therefore, it can be concluded that the doped Al and decorated Pt NPs provide additional electrons, thus broadening the band gap.

The specific surface areas of the nanoparticles were estimated from N_2 adsorption-desorption analysis. Fig. 6(b) shows the adsorption-desorption isotherms of the ZnO, AZO, Pt-ZnO, and Pt-AZO NPs. The Brunauer-Emmett-Teller (BET) specific surface areas of the nanoparticles were calculated from the N_2 adsorption branches to be ~ 33.6 , 34.7 , 41.2 , and 43.4 m^2/g for the ZnO, AZO, Pt-ZnO, and Pt-AZO NPs. The surface area of the AZO NPs is higher than that of the pure ZnO NPs owing to the decrease in the lattice volume of the AZO NPs when a Zn atom is replaced with a smaller Al atom, as discussed with regard to the XRD data in Fig. 2. In particular, the surface area of the Pt-AZO (Pt-ZnO) NPs increased considerably in comparison to that of the AZO (ZnO) NPs. This can be attributed to the attachment of the small Pt NPs with a high surface area on the AZO (ZnO) NP surface.

The activation energies (E_a) for the sensing responses of the sensors based on ZnO, AZO, Pt-ZnO, and Pt-AZO NPs in the operating temperature range of 350 – 450 $^\circ C$ were calculated. Fig. 6(c) shows the Arrhenius plots of the sensor responses for the ZnO, AZO, Pt-ZnO, and Pt-

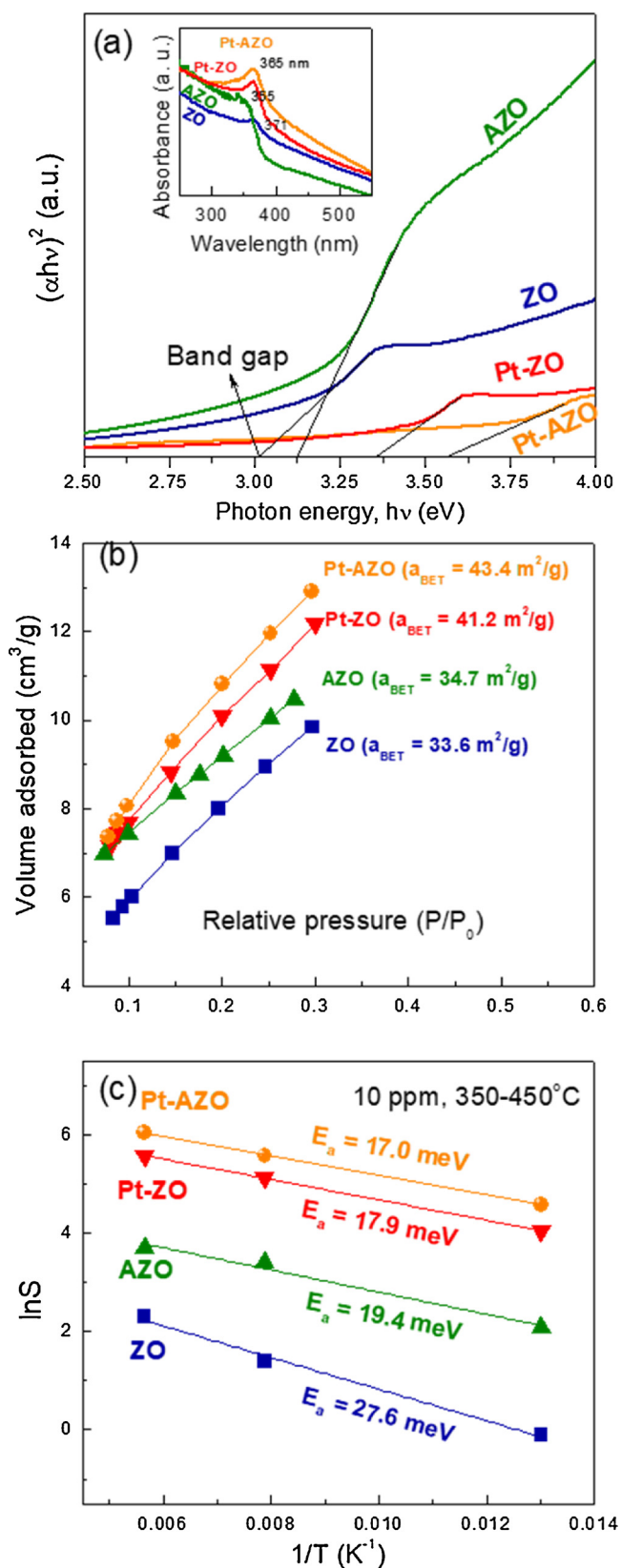
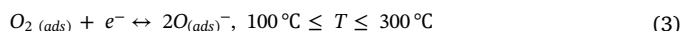


Fig. 6. (a) Optical band gaps of ZnO, AZO, Pt-ZnO, and Pt-AZO calculated from the UV-vis absorption spectra in the inset, (b) N_2 adsorption-desorption isotherms, and (c) Arrhenius plot, $\ln S$ versus $1/T$, for the sensing of 10 ppm acetone by ZnO, AZO, Pt-ZnO, and Pt-AZO sensing in the temperature range of 350–450 °C.

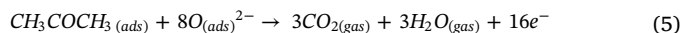
AZO NPs using the data in Fig. 3(b). The activation energies were estimated from the slopes of the best fits of the $\ln S$ versus $1/T$ plots in accordance with the Arrhenius' equation: $S = \exp(-E_a/(k_B T))$, where k_B is the Boltzmann constant. As shown in Fig. 6(c), the activation energies are 27.6, 19.4, 17.9, and 17.0 meV for the ZnO, AZO, Pt-ZnO, and Pt-AZO NPs, respectively. The E_a values decrease with Al-doping and also Pt NP decoration. The Pt-AZO NP thus has the lowest activation energy, which leads to faster surface chemical reactions, resulting in the best sensing properties.

Further, we analyze the effect of Pt on the sensing performance (observed in Figs. 3 and 4) of ZnO NPs by comparing the physical and chemical characteristics of the various particles (shown in Figs. 5 and 6). The sensing responses and response times are presented in Fig. 7(a) and (b), respectively. The activation energy, oxygen vacancies, band gap, and BET specific surface areas of the ZnO, AZO, Pt-ZnO, and Pt-AZO NPs are summarized in Fig. 7(c)–(f). The comparison between NPs without Pt, pure ZnO and AZO NPs, and those with Pt, Pt-ZnO and Pt-AZO NPs, reveals that both Al doping and the incorporation of Pt NPs on the surface increase the number of oxygen vacancies (Fig. 7(d)), optical band gap (Fig. 7(e)), and specific surface area (Fig. 7(f)) with respect to the initial state of materials. The improved properties (lower activation energy, Fig. 7(c)) lead to faster chemical reactions during the sensing procedure. Thus, a higher sensing response (Fig. 7(a)) and shorter response time (Fig. 7(b)) to acetone are observed with AZO NPs and Pt-AZO NPs compared to pure ZnO NPs and Pt-ZnO NPs, respectively. However, a noteworthy feature is that the significant enhancement in the sensing performance of ZnO NPs is due to the Pt catalyst on the surface rather than Al doping.

The sensing mechanism for acetone detection with various NPs is illustrated in Fig. 8. When the AZO NPs are exposed to air, which represents the initial state of the sensor, the oxygen molecules in air are adsorbed on the surface of the AZO NPs (Fig. 8(a), left; Eq. (1)). The adsorbed oxygen molecules trap the electrons from the conduction band of the AZO NPs and form anionic chemisorbed oxygen species (e.g., O_2^- , O^- , or O^{2-}), depending on the operating temperature, according to Eq. (2)–(4) [28]:



This leads to the formation of an electron depletion layer on the surface of the AZO NPs, which increases the resistance of the sensor. However, when the AZO NPs are exposed to acetone (CH_3COCH_3), the surface oxygen ion species react with acetone molecules, thus oxidizing it and releasing electrons back to the conduction band of the AZO NPs, as shown Fig. 8(a), right. At the working temperature of the AZO NPs of 500 °C, the O^{2-} species mainly interact with acetone, according to the following equation:



Consequently, a large number of electrons return back to the conduction band of AZO, resulting in a decrease in the thickness of the depletion layer, and therefore a decrease in the resistance of the AZO NPs.

Similarly, when the Pt-AZO NPs are exposed to air in the initial state (Fig. 8(b), left), adsorbed oxygen species are also formed on the surface of the Pt NPs and be easily dissociated into ionic oxygen species due to the spillover effect of the Pt metal (Fig. 8(b), left) [16]. Owing to the higher work function of the Pt metal than that of the AZO semiconductor, the electrons belonging to AZO are transferred to Pt [16]. This leads to enhanced dissociation of oxygen molecules into oxygen ions on the surface of the Pt NPs, which then easily diffuse to the

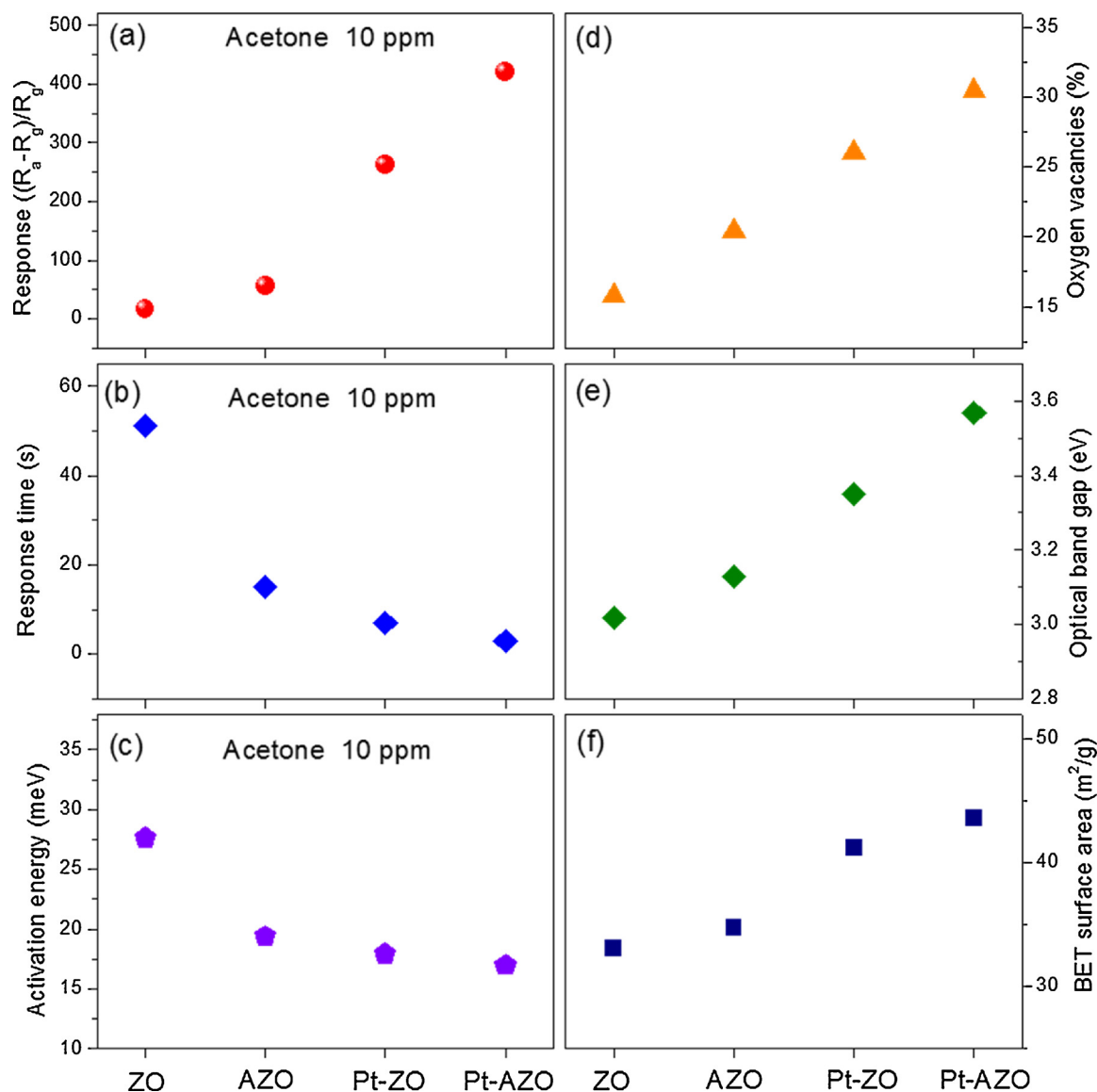


Fig. 7. Summary of the (a) sensing responses, (b) response times, (c) activation energies, (d) oxygen vacancies, (e) optical band gaps, and (f) BET surface areas of ZnO, AZO, Pt-ZnO, and Pt-AZO.

surface vacancies of the AZO NPs. Thus, the number of chemisorbed oxygen ion species is significantly increased, and additional active sites are created along with a thicker electron depletion layer at the interface between the Pt NPs and the AZO NPs. Thus, more reactive sites for acetone oxidation are created when the Pt-AZO NPs are exposed to acetone (Eq. (5); Fig. 8(b), right). In addition, the acetone molecules can efficiently adsorb on the Pt surface owing to the catalytic effect and can be easily transported to the adjacent AZO surface. Consequently, the oxidation of acetone occurs rather easily. Therefore, the significantly improved sensing performance of the Pt-AZO NPs can be attributed to the spillover effect and catalytic effect of the Pt NPs.

According to the sensing mechanism, the higher sensing performance is closely related to an increase in the thickness of the depletion layer in the initial state, resulting in a large number of adsorbed oxygen ions, thereby leading to a greater number of reactive sites for the target gas. More adsorbed oxygen ions are observed on the Pt-AZO NPs (Pt-ZnO) than on the AZO (ZnO) NPs (Fig. 7(d)), as indicated by the deconvoluted O 1s peaks in the XPS spectra (Fig. 5). The increased thickness of the electron depletion layer is caused by the increased number of electrons trapped in the oxygen molecules of the ZO NPs and AZO NPs at the surface of the materials. The donor Al atoms in the AZO

NPs can provide additional carriers compared to pure ZnO NPs. The Pt NPs in the Pt-ZO and Pt-AZO NPs can trap more electrons from the ZO and AZO NPs, respectively, owing to the higher work function of Pt compared to ZO and AZO. Therefore, both Al atoms and Pt NPs in Pt-AZO NPs supply more electrons to form a thicker depletion layer compared to Pt-ZO, AZO, and ZO, as confirmed by the increased band gap energies (Fig. 7(e)). In addition, when the Pt-AZO NPs are exposed to acetone, the acetone molecules can efficiently adsorb on the Pt surface of Pt-AZO NPs owing to the catalytic effect of Pt NPs and can be easily transported to the adjacent AZO surface. This is demonstrated in terms of two phenomena: the shortened response time (inset of Fig. 7(b)) and the enhanced kinetics of the surface reactions, as the activation energies of the Pt-ZnO and Pt-AZO NPs are lower than their counterparts without Pt (Fig. 7(c)). Thus, the significantly enhanced sensing performance of the Pt-AZO NPs can be attributed to the synergistic physical and chemical effects originating from the increase in the number of oxygen vacancies, optical band gap, specific surface area, and the enhanced reaction kinetics. Those increases arose from (i) the thicker depletion layer provided by the doping effect of Al donor and the spillover effect of Pt, and (ii) the catalytic effect of the Pt NPs during the acetone sensing reaction. However, Pt catalyst rather than Al

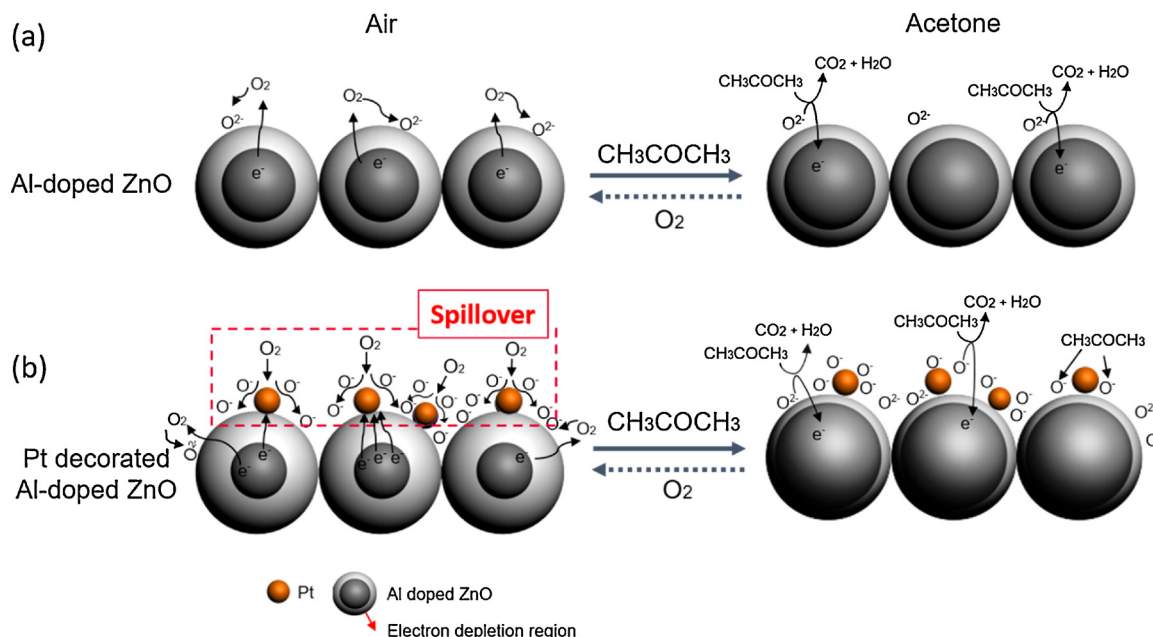


Fig. 8. Schematic illustrating the sensing reaction mechanism of (a) AZO and (b) Pt-AZO sensors in air and acetone.

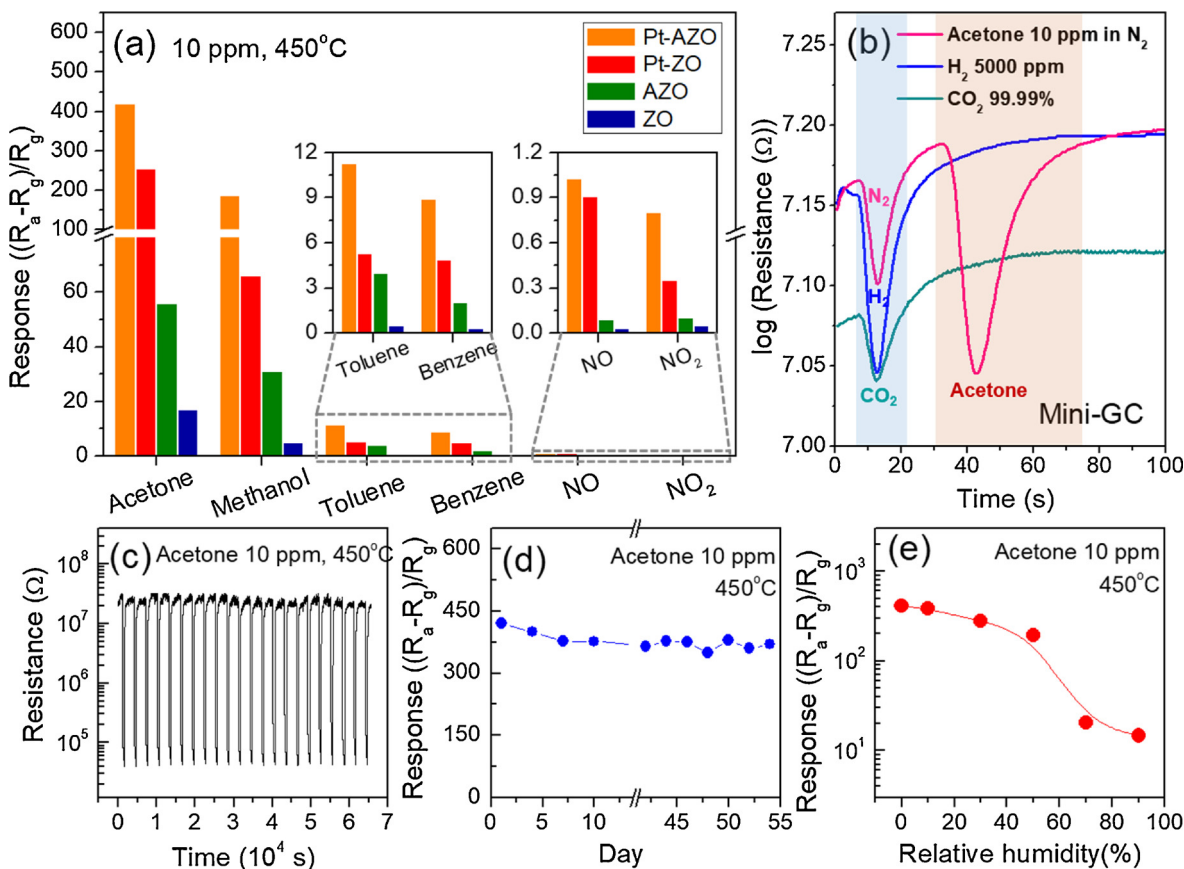


Fig. 9. (a) Responses of ZO, AZO, Pt-ZO, and Pt-AZO for 10 ppm of various target gases such as acetone, methanol, toluene, benzene, NO, and NO₂ at 450 °C, (b) selectivity of the ZnO NP-based sensor to detect acetone gas using a miniaturized gas chromatographic column [29]), (c) reliability of Pt-AZO in sensing 10 ppm acetone over 20 cycles at 450 °C, (d) stability of Pt-AZO exposed to 10 ppm acetone at 450 °C determined at an interval of 2–3 days, and (e) variation in the response of Pt-AZO for 10 ppm acetone as a function of relative humidity at 450 °C.

doping mainly contributes to the significant enhancement in the sensing performance of Pt-AZO NPs, as observed in our results.

Fig. 9 presents the sensing performance (selectivity, reproducibility, long-term stability, and humidity interference) of the Pt-AZO NPs to

10 ppm acetone at the optimal working temperature of 450 °C. Fig. 9(a) shows the response of the samples towards 10 ppm each of various gases, acetone, methanol, toluene, benzene, NO, and NO₂ gases at 450 °C. The insets of Fig. 9(a) show the magnified response plots for

Table 1
Comparison of the acetone-sensing properties of various types of metal-oxide-based sensors decorated with Pt.

Sensing materials	Operating Temperature [°C]	Concentration [ppm]	Response (R_a/R_g)	Sensitivity ^a [ppm^{-1}]	Response time [s]	Recovery time[s]	Ref.
Pt-decorated Al-doped ZnO NPs	450	10	421	42.1	2.9	440	This work
Pt-loaded porous WO ₃ NFs	350	5	121.5	24.1	< 32	–	[30]
Pt-loaded SnO ₂ NTs	350	5	93	18.4	> 120	–	[31]
Pt-decorated In ₂ O ₃ NPs	150	1.56	20	12.2	13	> 30	[32]
Pt-decorated SnO ₂ Fibers	300	3	3.5	0.83	15	< 6	[33]
Pt-decorated CuFe ₂ O ₄ NTs	300	100	17.5	0.16	–	350	[34]
Pt-functionalized NiO NTs	200	100	10	0.09	–	–	[35]
Pt-decorated SnO ₂ nanoflowers	100	50	3	0.04	–	–	[36]

^a sensitivity = response/concentration.

toluene, benzene, NO, and NO₂. The results indicate that all samples of ZO, AZO, Pt-ZO, and Pt-AZO NPs show a very high response for acetone compared to the other gases. Among the samples, the Pt-AZO NPs show the best sensing response to all gases. Recently, the selective sensing of acetone gas by a ZnO NP-based sensor was tested by a custom-made gas analyzing system, a miniaturized gas chromatographic column [29]. Fig. 9(b) shows the sensor responses of our ZnO NP-based sensor towards different target gases such as H₂, CO₂, and acetone. In the chromatograms, the peaks corresponding to the detection of H₂ (5000 ppm in synthetic air) and CO₂ (99.99%) appear close to 13 s. For 10 ppm acetone in nitrogen, two peaks are observed at 13 s and 42 s, corresponding to nitrogen and acetone gas, respectively. Thus, we confirmed that 10 ppm acetone can be separately detected using ZnO NP-based sensors.

Fig. 9(c) shows the reproducibility of Pt-AZO for sensing 10 ppm acetone over 20 cycles at 450 °C. The sensing resistance is almost constant for 20 cycles of gas input and release, which implies the good repeatability of the response of Pt-AZO NPs for 10 ppm acetone. Further, Fig. 9(d) shows the stability of Pt-AZO sensor with time under exposure to 10 ppm acetone, which was determined at an interval of 2–3 days for 54 days. The result indicates that during long-time continuous measurements, the sensor response remained almost stable, thus demonstrating the good stability of the Pt-AZO NPs. Fig. 9(e) shows the variation in the sensor response to 10 ppm acetone as a function of the relative humidity (RH) at 450 °C. The response decreases with an increase in the RH. However, at 50% RH, the sensing response of the Pt-AZO NPs to 10 ppm acetone is ~192, which is still higher compared to those of other materials. This implies that the Pt-AZO NPs are highly stable in humid conditions.

Further, we compare the acetone-sensing performance of Pt-AZO NPs with those of previously reported metal-oxide-based gas sensors incorporated with Pt [30–36]. The sensitivity of each sensing material is compared in terms of the ratio of the estimated response to the acetone concentration, as listed in Table 1. It is obvious that our sensor based on Pt-AZO NPs shows superior sensing performance both in terms of the sensitivity and response time

4. Conclusions

We carried out a comparative investigation on the acetone-sensing properties of pure ZnO, AZO, Pt-ZnO, and Pt-AZO NPs. The ZnO and AZO NPs were synthesized by a hydrothermal method and Pt NPs were homogeneously coated on their surfaces in an agitated vessel via a sputtering method. The sensor based on Pt-AZO NPs showed the best sensing response of ~421 and response time of ~2.9 s at the optimal working temperature of 450 °C under exposure to 10 ppm acetone. These sensing characteristics are remarkably better than those of sensors based on ZnO NPs (~17 and ~51 s, respectively), AZO NPs (~56 and ~15 s, respectively), and Pt-ZnO NPs (~261 and ~7 s, respectively). Significantly, the sensors based on Pt-decorated samples showed remarkably enhanced sensing performance for 10 ppm acetone

compared to the un-decorated samples. In particular, the significant improvement in the sensing properties is due to Pt decoration rather than Al doping. The Pt NPs on the surface of AZO NPs play a crucial role in improving the acetone-sensing performance. The spillover effect as the catalytic effect of the Pt NPs can be ascribed to the greater number of oxygen vacancies, higher carrier concentration, and larger specific surface area of the Pt-AZO NPs as compared to the bare AZO NPs, which provide more active adsorption sites and enhance the kinetics of the surface reactions. Furthermore, the sensing response of the sensor based on Pt-AZO NPs to 10 ppm acetone is superior to those of other previously reported acetone sensors based on semiconducting metal oxides. Therefore, the superior sensing performance of Pt-AZO NPs renders it suitable for practical application as an acetone-sensing material in environmental and industrial monitoring systems.

Acknowledgment

This research was supported by the Basic Science Research Program (2017M3A9F1052297) of the National Research Foundation of Korea (NRF) funded by the Ministry of Science, ICT & Future Planning.

Appendix A. Supplementary data

Supplementary material related to this article can be found, in the online version, at doi:<https://doi.org/10.1016/j.snb.2018.10.049>.

References

- [1] A. Mason, S.C. Mukhopadhyay, K.P. Jayasundera, Sensing technology: current status and future trends IV, *Smart Sens. Meas. Instrum.* 12 (2015) 2194–8402.
- [2] Q. Jia, H. Ji, Y. Zhang, Y. Chen, X. Sun, Z. Jin, Rapid and selective detection of acetone using hierarchical ZnO gassensor for hazardous odor markers application, *J. Hazard. Mater.* 276 (2014) 262–270.
- [3] P.W. Allen, H.J.M. Bowen, L.E. Sutton, O. Bastiansen, The molecular structure of acetone, *Trans. Faraday Soc.* 48 (1952) 991–995.
- [4] J.W. Gardner, H.W. Shin, E.L. Hines, An electronic nose system to diagnose illness, *Sens. Actuators B: Chem.* 70 (2000) 19–24.
- [5] M. Righettoni, A. Tricoli, S.E. Pratsinis, Si:WO₃ sensors for highly selective detection of acetone for easy diagnosis of diabetes by breath analysis, *Anal. Chem.* 82 (2010) 3581–3587.
- [6] C. Deng, J. Zhang, X. Yu, W. Zhang, X. Zhang, Determination of acetone in human breath by gas chromatography–mass spectrometry and solid-phase microextraction with on-fiber derivatization, *J. Chromatogr. B* 810 (2004) 269–275.
- [7] S.V. Ryabtsev, A.V. Shaposhnick, A.N. Lukin, E.P. Domashevskaya, Application of semiconductor gas sensors for medical diagnostics, *Sens. Actuators B: Chem.* 59 (1999) 26–29.
- [8] S.M. Kanan, O.M. El-Kadri, I.A. Abu-Yousef, M.C. Kanan, Semiconducting metal oxide based sensors for selective gas pollutant detection, *Sensors* 9 (2009) 8158–8196.
- [9] P.P. Sahay, Zinc oxide thin film gas sensor for detection of acetone, *J. Mater. Sci.* 40 (2005) 4383–4385.
- [10] T.-R. Rashid, D.-T. Phan, G.-S. Chung, A flexible hydrogen sensor based on Pd nanoparticles decorated ZnO nanorods grown on polyimide tape, *Sens. Actuators B: Chem.* 185 (2013) 777–784.
- [11] V. Galstyan, E. Comini, C. Baratto, G. Faglia, M. Brisotto, E. Bontempi, G. Sberveglieri, Growth and gas sensing properties of rough ZnO nanowires, *Proceedings of the IMCS, 14th International Meeting on Chemical Sensors*, (2012), pp. 1623–1625.
- [12] Y. Xiao, L. Lu, A. Zhang, Y. Zhang, L. Sun, L. Huo, F. Li, Highly enhanced acetone

- sensing performances of porous and single crystalline ZnO nanosheets: high percentage of exposed (100) facets working together with surface modification with Pd nanoparticles, *ACS Appl. Mater. Interfaces* 4 (2012) 3797–3804.
- [13] X. Yu, F. Song, B. Zhai, C. Zheng, Y. Wang, Electro spun ZnO nanotubes and its gas sensing applications, *Phys. E: Low-Dimens. Syst. Nanostruct.* 52 (2013) 92–96.
- [14] S.B. Khan, M. Faisal, M.M. Rahman, A. Jamal, Low-temperature growth of ZnO nanoparticles: photocatalyst and acetone sensor, *Talanta* 85 (2011) 943–949.
- [15] L. Wang, S. Wang, M. Xu, X. Hu, H. Zhang, Y. Wang, W. Huang, A Au-functionalized ZnO nanowire gas sensor for detection of benzene and toluene, *Phys. Chem. Chem. Phys.* 15 (2013) 17179–17186.
- [16] A.A. Daryakenari, A. Apostoluk, J.-J. Delaunay, Effect of Pt decoration on the gas response of ZnO nanoparticles, *Phys. Status Solidi C* 10 (2013) 1297–1300.
- [17] S. Bai, S. Chen, Y. Zhao, T. Guo, R. Luo, D. Li, A. Chen, Gas sensing properties of Cd-doped ZnO nanofibers synthesized by the electrospinning method, *J. Mater. Chem. A* 2 (2014) 16697–16706.
- [18] N.H. Al-Hardana, M.J. Abdullah, A. Abdul Aziz, Performance of Cr-doped ZnO for acetone sensing, *Appl. Surf. Sci.* 270 (480) (2013) 485.
- [19] M.H. Darvishnejad, A.A. Firooz, J. Beheshtian, A.A. Khodadadi, Highly sensitive and selective ethanol and acetone gas sensors by adding some dopants (Mn, Fe, Co, Ni) onto hexagonal ZnO plates, *RSC Adv.* 6 (2016) 7838–7845.
- [20] Y.-S. Shim, H.G. Moon, D.H. Kim, L. Zhang, S.-J. Yoon, Y.S. Yoon, C.-Y. Kang, H.W. Jang, Au-decorated WO₃ cross-linked nanodomains for ultrahigh sensitive and selective sensing of NO₂ and C₂H₅OH, *RSC Adv.* 3 (2013) 10452–10459.
- [21] R. Yoo, S. Cho, M.-J. Song, W. Lee, Highly sensitive gas sensor based on Al-doped ZnO nanoparticles for detection of dimethyl methylphosphonate as a chemical warfare agent simulant, *Sens. Actuators B: Chem.* 221 (2015) 217–223.
- [22] R. Yoo, D. Lee, S. Cho, W. Lee, Doping effect on the sensing properties of ZnO nanoparticles for detection of 2-chloroethyl ethylsulfide as a mustard simulant, *Sens. Actuators B: Chem.* 254 (2018) 1242–1248.
- [23] L.-J. Bie, X.-N. Yan, J. Yin, Y.-Q. Duan, Z.-H. Yuan, Nanopillar ZnO gas sensor for hydrogen and ethanol, *Sens. Actuators B: Chem.* 126 (2007) 604–608.
- [24] J. Wang, Y. Li, Y. Kong, J. Zhou, J. Wu, X. Wu, W. Qin, Z. Jiao, L. Jiang, Non-fluorinated superhydrophobic and micro/nano hierarchical Al doped ZnO film: the effect of Al doping on morphological and hydrophobic properties, *RSC Adv.* 5 (2015) 81024–81029.
- [25] B.E. Sernelius, K.F. Berggren, Z.C. Jin, I. Hamberg, C.G. Granqvist, P band-gap tailoring of ZnO by means of heavy Al doping, *Phys. Rev. B* 37 (1988) 10244–10248.
- [26] J. Tauc, *Amorphous and Liquid Semiconductors*, Plenum Press, New York, 1974, p. 171.
- [27] R.S. Weber, Effect of local structure on the UV-visible absorption edges of molybdenum oxide clusters and supported molybdenum oxides, *J. Catal.* 151 (1995) 470–474.
- [28] Z. Ahmad, A.Z. Sadek, K. Latham, J. Kita, R. Moos, W. Wlodarski, Chemically synthesized one-dimensional zinc oxide nanorods for ethanol sensing, *Sens. Actuators B: Chem.* 187 (2013) 295–300.
- [29] H. Jung, W. Cho, R. Yoo, H.-S. Lee, Y.-S. Choe, J.Y. Jeon, W. Lee, Highly selective real-time detection of breath acetone by using ZnO quantum dots with a miniaturized gas chromatographic column, *Sens. Actuators B: Chem.* 274 (2018) 527–532.
- [30] S.-J. Choi, S.-J. Kim, W.-T. Koo, H.-J. Cho, I.-D. Kim, Catalyst-loaded porous WO₃ nanofibers using catalyst-decorated polystyrene colloid templates for detection of biomarker molecules, *Chem. Commun.* 51 (2015) 2609–2612.
- [31] J.-S. Jang, S.-J. Kim, S.-J. Choi, N.-H. Kim, M. Hakim, A. Rothschild, I.-D. Kim, Thin-walled SnO₂ nanotubes functionalized with Pt and Au catalysts via the protein templating route and their selective detection of acetone and hydrogen sulfide molecules, *Nanoscale* 7 (2015) 16417–16426.
- [32] M. Karmaoui, S.G. Leonardi, M. Latino, D.M. Tobaldi, N. Donato, R.C. Pullara, M.P. Seabra, J.A. Labrincha, G. Neri, Pt-decorated In₂O₃ nanoparticles and their ability as a highly sensitive (< 10 ppb) acetone sensor for biomedical applications, *Sens. Actuators B: Chem.* 230 (2016) 697–705.
- [33] J. Shin, S.-J. Choi, I. Lee, D.-Y. Youn, C.O. Park, J.-H. Lee, H.L. Tuller, I.-D. Kim, Thin-wall assembled SnO₂ fibers functionalized by catalytic Pt nanoparticles and their superior exhaled-breath-sensing properties for the diagnosis of diabetes, *Adv. Funct. Mater.* 23 (2013) 2357–2367.
- [34] C. Zhao, W. Lan, H. Gong, J. Bai, R. Ramachandran, S. Liu, F. Wang, Highly sensitive acetone-sensing properties of Pt-decorated CuFe₂O₄ nanotubes prepared by electrospinning, *Ceram. Int.* 44 (2018) 2856–2863.
- [35] J. Fu, C. Zhao, J. Zhang, Y. Peng, E. Xie, Enhanced gas sensing performance of electrospun Pt-functionalized NiO nanotubes with chemical and electronic sensitization, *ACS Appl. Mater. Interfaces* 5 (2013) 7410–7416.
- [36] L. Wang, Y. Wang, K. Yu, S. Wang, Y. Zhang, C. Wei, A novel low temperature gas sensor based on Pt-decorated hierarchical 3D SnO₂ nanocomposites, *Sens. Actuators B: Chem.* 232 (2016) 91–101.

Ran Yoo received her Ph.D. from the Department of Materials and Engineering in Yonsei University in 2018. She is currently studying on the enhancement gas sensing properties using modification of nanostructured metal oxide.

Hyun-Sook Lee received her Ph.D. from the Department of Physics of POSTECH in 2008. Now she is a research professor in the Department of Materials Science and Engineering of Yonsei University from 2015. Her research interests are various materials related in high-temperature superconductivity, solid-state hydrogen storage, rare-earth/rare-earth-free permanent magnets, nanostructured metal oxide semiconductor gas sensors, and nanostructured thermoelectrics.

Wooyoung Lee is a Professor of Department of Materials Science and Engineering at Yonsei University in Korea. He received a BS degree in metallurgical engineering from the Yonsei University in 1986, a MS degree in metallurgical engineering from the Yonsei University in 1988. He received a Ph.D. degree in Physics from University of Cambridge, England in 2000. He is also the Chairman in University Industrial Technology Force (UNITEF), and a Member of the National Council on Science and Technology. In recent years, his research interests have centered on thermoelectric devices, spintronics and hydrogen sensors based on nanowires. He has received a number of awards in nano device-related research areas, including a Service Merit Medal (2008) due to contribution on the development of intellectual properties. He has authored and co-authored over 150 publications, and has edited a few of special books on nano-structured materials and device.